Editors' Suggestion | Featured in Physics

Rotation-Time Symmetry Breaking in Frustrated Chiral Nematic Driven by a Pulse-Train Waveform

Vitaly P. Panov,[1,*] Jiseon Yang,[1] L. K. Migara,[2] Hyun-Jin Yoon,[1,3] and Jang-Kun Song[1,†]
[1]Department of Electrical and Computer Engineering, Sungkyunkwan University, Suwon, Gyeonggi-do 16419, Republic of Korea
[2]School of Engineering, Sri Lanka Technology Campus, Padukka 10500, Sri Lanka
[3]Merck Performance Materials Ltd., Pyeongtaek 17956, Republic of Korea

(Received 31 December 2021; revised 3 July 2022; accepted 5 August 2022; published 9 September 2022)

We report waveform-induced rotation-time symmetry breaking in liquid crystal director motion. Homeotropic cells filled with a negative dielectric anisotropy chiral nematic exhibit persistent and visually observable waves of director orientation with a time period of at least 30 driving field cycles. Their existence in the space of driving waveform parameters is explored. The possibility of utilizing this system, which exhibits both spatial and temporal long-range order, as a modeling tool for experimental studies on discrete time crystals is discussed.

DOI: 10.1103/PhysRevLett.129.117801

Liquid crystals (LCs) are widely used in displays and other applications owing to their orientational order and fluidity. In the nematic (N) LC phase, rodlike molecules are, on average, parallel to a pseudovector $\boldsymbol{n}$ defined as the director. Spatial variation of the director induced by a confining geometry, chirality, and external fields [1–7] can cause LC materials to form various observable patterns. These patterns often indicate spontaneous symmetry breaking [8–10].

Standing waves with self-adaptation to driving frequencies have recently been discovered in homeotropic sandwich cells filled with negative dielectric anisotropy chiral nematics [11,12]. Exotic matter states involving topological transitions have also been reported in the system [13].

In this Letter, we demonstrate traveling waves that can be induced in a frustrated chiral nematic system by breaking the rotation-time symmetry of a LC director. The waves appear on the application of pulse-train waveforms [Fig. 1(a)] to the above type of cells. Time-dependent patterns are caused by changes in the azimuthal angle φ of the nematic director with each cycle of the applied voltage [Fig. 1(b)], as verified by the 2000 frames/s conoscopic observations [Fig. 1(c) and Supplemental Material [14], video "FastConoscopy"].

When the sample is placed between crossed polarizers with a backlight, the waves are observable to the naked eye as constantly moving dark and bright brushes [Figs. 1(d) and 1(e) and the Supplemental Material [14] videos]. After a short stabilization period, the wave pattern movement continues indefinitely.

The LC material used in this study (commercial nematic mixture MLC-7026-000, Merck Co., Korea) exhibits negative dielectric anisotropy ($\Delta\epsilon = -3.9$), which leads to the Fréedericksz transition [15] under moderate voltages. The given concentration (0.2 wt.%) of the chiral dopant (R811, Merck Co., Korea, helical twisting power 11 μm^{-1}) corresponds to a helical pitch of approximately 45 μm, which is greater than 10 times the cell gap (3.5 μm). Thus, the LC had a uniform surface-stabilized homeotropic alignment [16] (i.e., a frustrated chiral system), confirmed by a perfect dark state between the crossed polarizers. A wedge cell experiment (Supplemental Material [14], video "Wedge") shows significant slowdown (suppression) of the phenomenon for thicknesses greater than 5–10 μm. The chiral dopant concentration is proven to be a critical parameter as no traveling waves can be found in pure achiral LCs or in mixtures with chiral dopant concentrations above 0.5 wt.%.

A continuous change in the tilt direction is observed when $1.5 < (t_{OFF}/\tau_{OFF}) < 3.0$. Here $\tau_{OFF} = 8.2$ ms denotes the sample switching time, and the waveform parameters [defined in Fig. 1(a)] are $A_{ON} = 7$ V, $t_{ON} = 4$ ms, and $\psi_{sq} = 0°$. A longer t_{OFF} or faster τ_{OFF} would result in complete recovery of the homeotropic alignment during t_{OFF}, and the previous tilt direction would be "forgotten." A lower (t_{OFF}/τ_{OFF}) would result in a stable planar state.

The rotation of the director occurs in small droplets of the mixture surrounded by the positive $\Delta\epsilon$ LC material 4-cyano-4'-pentylbiphenyl (see Supplemental Material [14], video "SmallDrops"), implying that the sample area exerts no influence. This is intrinsically different from the self-adjustment to sample geometry of standing waves in the same mixture [11]. The traveling waves generate no physical flow; otherwise, the two fluids would mix rapidly. However, we cannot exclude the significance of local backflow generated during the Fréedericksz transition.

Bunches of threadlike defects and schlieren textures can be found near the electrode edges and nodal points of the wave pattern. The director rotation is also visible in the schlieren texture areas (Supplemental Material [14],

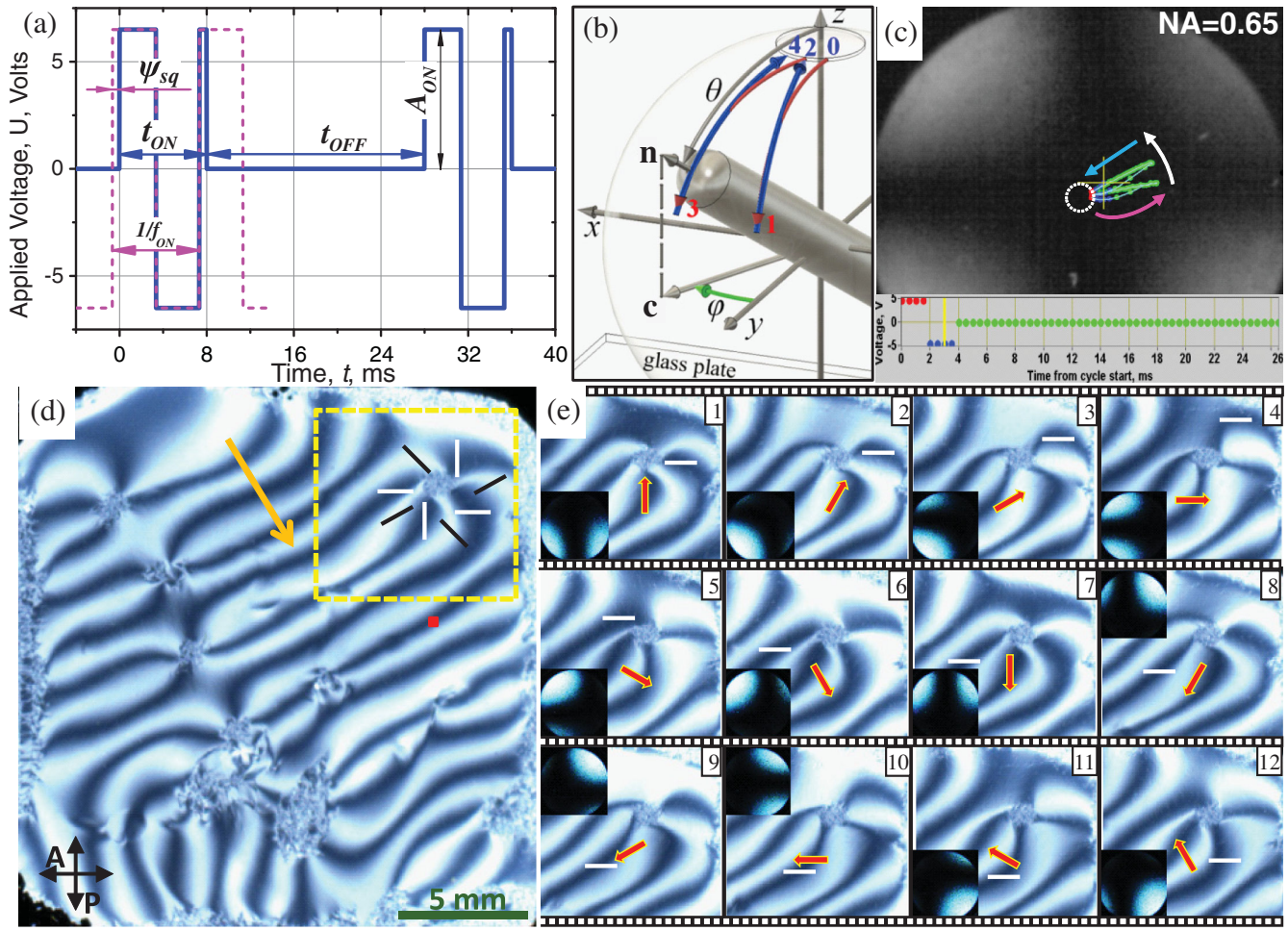

FIG. 1. (a) Definition of the waveform (thick blue line) parameters: signal period $= t_{ON} + t_{OFF}$; phase ψ_{sq} of the square wave (dashed magenta line, $\psi_{sq} = 30°$) is set at the beginning of each t_{ON} time interval. When the square wave frequency f_{ON} is an integral multiple of $1/t_{ON}$, the average dc is zero. (b) Coordinates describing LC director ($\boldsymbol{n}$) motion (…–0–1–2–3–4–…): the z axis is normal to the substrates; $\boldsymbol{c}$, projection of $\boldsymbol{n}$ on sample plane xy; θ, polar angle; and φ, azimuthal angle. The sphere is an eye guide. During t_{ON}, the electric field is applied along the z axis; because $\Delta\epsilon < 0$, $\boldsymbol{n}$ starts tilting away from the vertical position, following red paths (0–1, 2–3, etc.). During t_{OFF}, the elastic forces return the director to a nearly (limited by finite t_{OFF}) vertical alignment state following different paths (blue, 1–2, 3–4, etc.). (c) Conoscopic observation: the difference between ON (curved magenta arrow) and OFF (straight teal arrow) motion paths of the melatope is visible. A minimum tilt of ~1° always remains (dotted circle). (d) Traveling wave pattern in a LC cell between crossed polarizers. Orange arrow depicts the wave propagation direction. The white and black lines designate $\boldsymbol{c}$ parallel and/or perpendicular or at ±45° to the polarizer. The red square represents the light-emitting diode (LED) projection on the sample [Fig. 2(a)]. (e) Temporal evolution of the pattern (Supplemental Material [14], "WavesVideo"). Every third cycle of input waveform is shown. $A_{ON} = 6.0$ V, $\psi_{sq} = 0°$, $t_{ON} = 10$ ms, $t_{OFF} = 23.3$ ms, $f_{ON} = 100$ Hz. The red arrows and conoscopic images in the insets depict azimuthal angle evolution at a single point.

video "Defects" and image "wdef"), indicating that the phenomenon under consideration is independent of the defects. However, research on the combined behavior of traveling waves and defect patterns could be an intriguing future challenge.

The light transmittance between the crossed polarizers at a single spot was recorded as a function of time [Fig. 2(a)] to investigate the behavior of the director orientation as a function of the applied waveform parameters. A fragment of this dataset is shown in Fig. 2(b). Each cycle of the input waveform generates a peak in the transmittance: the peak intensity dependent on the azimuthal angle φ of the tilt. When the polarizer and analyzer are aligned with the x and y axes, respectively [Fig. 1(b)], the tilting directions near $\varphi = 45°$, 135°, 225°, and 315° produce maximum intensities, allowing us to determine the period $1/f_{360}$ of the full-cycle evolution of the azimuthal angle [Fig. 2(b)].

The fast Fourier transform (FFT) of the optical transmittance data is shown in Fig. 2(c). The high-frequency range of the response is occupied by components of the Fréedericksz transition switching under the applied waveform. These peaks are split due to the transmittance

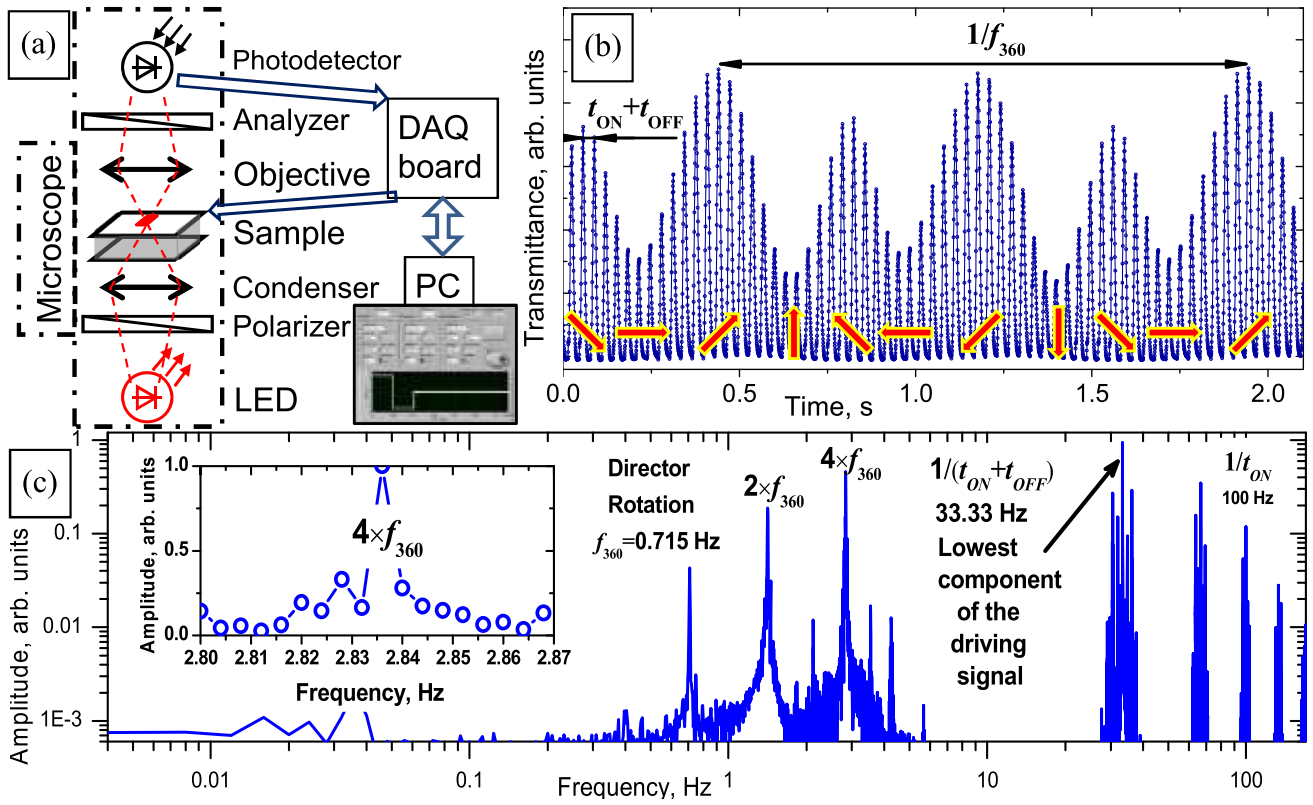

FIG. 2. (a) Schematic diagram of the setup for time periodicity studies of patterns. (b) Fragment of a typical signal. The red arrows indicate the change in the tilt direction with wave propagation. (c) FFT spectrum of the transmittance for $A_{ON} = 5.2$ V, $\psi_{sq} = 0°$, $t_{ON} = 10$ ms, $t_{OFF} = 20$ ms, $f_{ON} = 100$ Hz. Inset: magnified peak at $4 \times f_{360}$.

modulation by the periodic change in the azimuthal angle φ. The change in the azimuthal angle generates peaks below the lowest frequency $[1/(t_{ON} + t_{OFF})]$ existing in the driving signal. Owing to the fourfold symmetry of crossed polarizers, the strongest peak corresponds to a 90° change in the azimuthal angle φ, i.e., a quarter of the complete cycle. As the maximum director tilt θ_{max} is dependent on φ, subharmonics $2 \times f_{360}$ and f_{360} are also present. Low noise values in the low-frequency range and narrow peaks corresponding to the azimuthal change of the director [Fig. 2(c), inset] indicate the temporal stability of the LC director rotation over a longer period than the measurement duration (250 s).

To determine the range of the input waveform parameters leading to the generation of traveling waves, we mapped f_{360} as a function of t_{OFF}, t_{ON}, and A_{ON} using the aforementioned experimental setup. A well-defined triangle can be observed on the t_{OFF}/A_{ON} plane (Fig. 3), where the traveling wave can be detected. This area is limited by the insufficient average electric field for the Fréedericksz transition on the left and bottom sides and by the "standing wave" patterns [11] on the top right side (Supplemental Material [14], video "VoltDep"). The maximum value of f_{360} is obtained just above the Fréedericksz transition threshold voltage, where the **c** director makes a complete turn in less than 1 s. Therefore, a major change in the azimuthal angle occurs near the vertical alignment. A discernible change in the azimuthal angle per waveform cycle of up to $\Delta\varphi \approx 12°$ can be observed [Fig. 3(b)]. The dependence of $\Delta\varphi$ on t_{OFF} demonstrate the appearance, gradual increase in speed, and abrupt vanishing of the traveling wave phenomenon with t_{OFF}.

In comparison, t_{ON} appears to exert less influence on the azimuthal rotation of the director once the electric field and t_{ON} become sufficient for LC switching (Supplemental Material [14], Fig. S2).

The dependence of the wave frequency on the square wave ψ_{sq} [defined in Fig. 1(a)] demonstrates a remarkably linear decline of f_{360} over most of the range and a rapid decrease to zero (i.e., no traveling waves) just before 180° and 360° (Fig. 4). The maximum wave frequency can be found when the ψ_{sq} was either 0° or 180° and $f_{ON} = 1/t_{ON}$. For higher values of f_{ON}, the waves move slower, and their existence ranges are narrower. Interestingly, changing the ψ_{sq} of the input waveform by 180° instantly reverses the propagation direction of the waves (Fig. 4, insets, Supplemental Material [14], video "Reverse"), indicating the polar nature of the phenomenon, which is likely linked to the presence of flexoelectric polarization.

Meanwhile, the high-speed conoscopic imaging (Supplemental Material [14], video "FastConoscopy") shows an increase in the apparent polar angle for a few

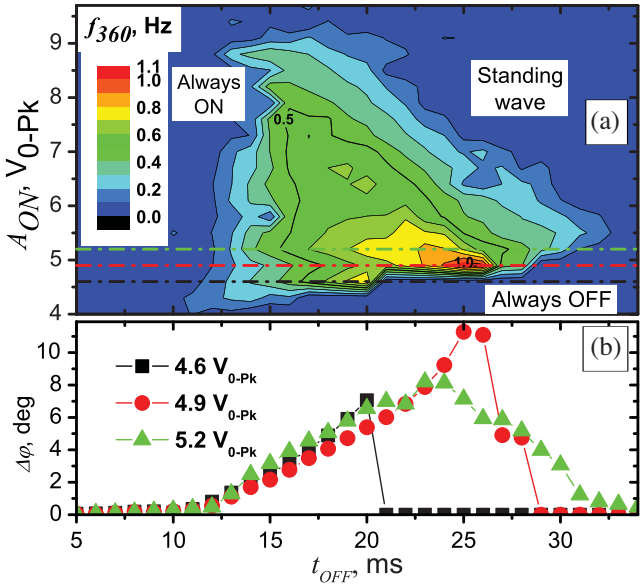

FIG. 3. (a) Dependence of the rotation frequency f_{360} of the **c** director on the amplitude of the applied voltage A_{ON} and OFF time t_{OFF}. Experimental parameters are $t_{ON} = 4$ ms, $f_{ON} = 250$ Hz, $\psi_{sq} = 0°$, settling time = 100 s/point, acquisition time = 250 s/point. (b) Cross-sectional profiles corresponding to three values of A_{ON} [dash-dotted lines of corresponding colors on (a)], near the maximum of f_{360}. The frequency is converted into a variation in the azimuthal angle $\Delta\varphi$ per cycle of applied waveform.

milliseconds after the voltage is set to zero. This indicates that mobile ions have an important role. Moreover, the effects of flexoelectricity and ions may be practically indistinguishable [17]. Under certain conditions, ions in ac fields can cause convection via an electrokinetic effect [18]. However, we did not observe any regular motion of particles floating in the LC sample.

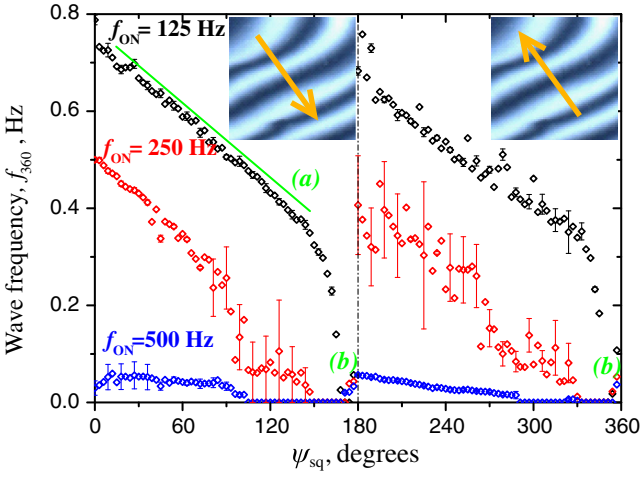

FIG. 4. Dependence of the rotation frequency f_{360} the **c** director on the ψ_{sq} parameter of applied pulse train and square wave frequency f_{ON}. $t_{ON} = 8$ ms, $t_{OFF} = 22$ ms, $A_{ON} = 6.2$ V, settling time = 200 s/point, acquisition time = 250 s/point. A linear decline in the frequency for most of the ψ_{sq} range [green line (a)] and regions with no movement (b) was observed. Crossing $\psi_{sq} = 180°$ results in change of the movement direction (orange arrows on the insets).

The response of the wave frequency to the change in the ψ_{sq} of the square wave indicates that rapid change in the azimuthal angle occurs immediately after the application of the electric field, i.e., when the polar angle θ is relatively small and the alignment is nearly homeotropic. This observation is in accordance with our findings obtained from the conoscopic observations and voltage-dependence experiments [Figs. 1(c) and 3]. Further analysis of the azimuthal angle as a function of ψ_{sq} can be performed using Duhamel's principle [19]. However, the highly nonlinear nature of LC switching requires further work based on nonlinear dynamical models, such as the Volterra series [20,21].

The wave behavior can be determined based on the delicate interplay of the three time constants: τ_{OFF} and τ_{ON} of the Fréedericksz transition and $\tau_{helix} \propto (\gamma p^2)/K$ of the electric field–helical structure flexoelectric interaction [22,23], where γ denotes the viscosity, p denotes the helical pitch, and K denotes the elastic constant. In the completely switched ON and OFF states, the helix in the chiral nematic was suppressed. However, during the switching process, when the contributions of the surface, electric field, and viscosity are balanced, the elastic forces can partially recreate the helix for a short time. In this case, the helical axis is at an oblique angle to the sample plane; the flexoelectricity deviates the axis, resulting in a change in the average azimuthal angle φ [22]. The positive and negative half waves of the electric field cause an opposite change in φ. Because the Fréedericksz transition is in progress, the positive and negative half waves fall on different values of the polar angle θ. Furthermore, the polar angle switches back without a significant change in φ during the off time. Therefore, the net deviation over the waveform cycle is not zero, and the azimuthal rotation symmetry is broken.

In contrast to other widely used periodic signals (sine, square, etc.), the temporal symmetry of the pulse-train waveform is broken for most of the ψ_{sq} values ($\psi_{sq} \neq \pm 90°$); that is, $U(t - t_0) \neq U[-(t - t_0)]$ regardless of the arbitrary shift t_0. A combination of this symmetry breaking with the broken chiral symmetry of our system leads to the observed director rotation. Moreover, the elastic interaction within the material stabilized the change in the azimuthal angle across the sample plane, resulting in a wavelike appearance of the LC director pattern [Fig. 1(d)]. This can be classified as space-time symmetry breaking and resembles the behavior of time crystals [24]. Although the ideal time crystals are forbidden by the thermodynamic laws [25], if periodic external driving is allowed, discrete time crystals possessing (i) longer periods of oscillations than the driving force, (ii) no entropy generation, and (iii) long-range order are possible [26] and

have been reported [27–29]. For comparison, in our case, (i) $1/f_{360} \approx 1.4$ s is over 40 times $(t_{ON} + t_{OFF}) = 0.03$ s [Fig. 2(c)], (ii) no energy variance exists between the different azimuthal positions of the LC director, and (iii) the oscillations remain coherent over at least the sample size (20 mm) and duration of the experiment (hundreds of director rotation cycles). The wavelength is significantly longer than the other characteristic dimensions of the system (helical pitch and sample thickness). Therefore, this relatively simple approach could serve as a promising experimental platform for exploring time crystals' properties [27,28].

In electrodynamics or acoustics, a standing wave represents a special case of a traveling wave corresponding to an exact match between the wavelength and boundary conditions. By contrast, the standing wave reported by Migara and Song [11] is not a special case of the traveling waves considered here: these represent two separate phase states, each existing within its own range of input parameters (Supplemental Material [14], video "VoltDep") and corresponding to the topological crystalline [13] and "time crystal" states, respectively.

In summary, we report the observation of traveling waves resulting from director reorientation in liquid crystalline samples, which is associated with rotation-time symmetry breaking in response to pulse-train waveforms. Furthermore, we propose to investigate other known dynamic LC systems [1,30–34] for temporal symmetry breaking and the presence of other exotic states of matter [13,35]. A possibility of controlling the traveling waves by changing the applied signal parameters is demonstrated. Notably, both polar and azimuthal angles of the LC director can be controlled via an application of the field along just a single axis. This is important for potential applications, possibly leading to new approaches in LC director manipulation, colloidal assembly [11], and singular optics [12,36].

We are grateful to A. V. Dubtsov, J. K. Vij, D. N. Sidorov, A. V. Emelyanenko, S. A. Shvetsov, and S.-H. Hong for fruitful discussions. This research was supported by the National Research Foundation of Korea (NRF) funded by the Ministry of Science and ICT (NRF-2019R1A2C2008359) and by the ICT Creative Consilience program (IITP-2020-0-01821). V. P. was supported through the Brain Pool Program (NRF-2019H1D3A2A02060963) and Creative Challenge projects No. (NRF-2020R1I1A1A01072707, No. NRF-2021R1I1A1A01061278).

*vpanov@skku.edu
†Corresponding author.
jk.song@g.skku.edu

[1] A. Buka and L. Kramer, *Pattern Formation in Liquid Crystals* (Springer-Verlag, New York, NY, 2013), ISBN: 9781461284642.
[2] J. W. Goodby, P. J. Collings, T. Kato, C. Tschierske, H. F. Gleeson, and P. Raynes, *Handbook of Liquid Crystals* (Wiley VCH, Weinheim, 2014), ISBN: 9783527327737, 10.1002/9783527671403.
[3] I. Dierking, *Textures of Liquid Crystals* (John Wiley & Sons, New York, 2006), ISBN: 3527605274, 9783527605279.
[4] P. J. Ackerman, T. Boyle, and I. I. Smalyukh, Squirming motion of baby skyrmions in nematic fluids, Nat. Commun. **8**, 673 (2017).
[5] S. Shvetsov, T. Orlova, A. V. Emelyanenko, and A. Zolot'ko, Thermo-optical generation of particle-like structures in frustrated chiral nematic film, Crystals **9**, 574 (2019).
[6] A. J. Hurd, S. Fraden, F. Lonberg, and R. B. Meyer, Field-induced transient periodic structures in nematic liquid crystals: The splay Frederiks transition, J. Phys. (Paris) **46**, 905 (1985).
[7] S. Aya and F. Araoka, Kinetics of motile solitons in nematic liquid crystals, Nat. Commun. **11**, 3248 (2020).
[8] J. V. Selinger, Z. G. Wang, R. F. Bruinsma, and C. M. Knobler, Chiral Symmetry-Breaking in Langmuir Monolayers and Smectic Films, Phys. Rev. Lett. **70**, 1139 (1993).
[9] V. P. Panov, R. Balachandran, J. K. Vij, M. G. Tamba, A. Kohlmeier, and G. H. Mehl, Field-induced periodic chiral pattern in the N_x phase of achiral bimesogens, Appl. Phys. Lett. **101**, 234106 (2012).
[10] V. P. Panov, M. Nagaraj, J. K. Vij, Yu. P. Panarin, A. Kohlmeier, M. G. Tamba, R. A. Lewis, and G. H. Mehl, Spontaneous Periodic Deformations in Nonchiral Planar-Aligned Bimesogens with a Nematic-Nematic Transition and a Negative Elastic Constant, Phys. Rev. Lett. **105**, 167801 (2010).
[11] L. K. Migara and J.-K. Song, Standing wave-mediated molecular reorientation and spontaneous formation of tunable, concentric defect arrays in liquid crystal cells, NPG Asia Mater. **10**, e459 (2018).
[12] L. K. Migara, H. Lee, C.-M. Lee, K. Kwak, D. Lee, and J.-K. Song, External pressure induced liquid crystal defects for optical vortex generation, Curr. Appl. Phys. **18**, 819 (2018).
[13] M. G. Clerc, M. Kowalczyk, and V. Zambra, Topological transitions in an oscillatory driven liquid crystal cell, Sci. Rep. **10**, 19324 (2020).
[14] See Supplemental Material at http://link.aps.org/supplemental/10.1103/PhysRevLett.129.117801 for details of the experimental procedures, additional data, images and videos.
[15] V. Fréedericksz and A. Repiewa, Theoretisches und Experimentelles zur Fragenach der Natur der anisotropen Flüssigkeiten, Z. Phys. **42**, 532 (1927).
[16] B. Zeldovich and N. Tabiryan, Fréedericksz transition in cholesteric liquid-crystals without external fields, JETP Lett. **34**, 406 (1981), http://jetpletters.ru/ps/1520/article_23226.pdf.
[17] S. L. Cornford, T. S. Taphouse, and J. R. Sambles, Analysis of the sign-dependent switching observed in a hybrid aligned nematic cell, New J. Phys. **11**, 013045 (2009).
[18] C. Peng, Y. Guo, C. Conklin, J. Viñals, S. V. Shiyanovskii, Q.-H. Wei, and O. D. Lavrentovich, Liquid crystals with

patterned molecular orientation as an electrolytic active medium, Phys. Rev. E **92**, 052502 (2015).
[19] Fritz John, *Partial Differential Equations*, 4th ed. (Springer-Verlag, New York, 1982), ISBN: 0387906096.
[20] D. N. Sidorov, *Integral Dynamical Models: Singularities, Signals and Control*, World Scientific Series on Nonlinear Science Series A Vol. 87 (World Scientific, Singapore, 2014), ISBN: 9814619205, 9789814619202.
[21] D. N. Sidorov and N. A. Sidorov, Convex majorants method in the theory of nonlinear Volterra equations, Banach J. Math. Anal. **6**, 1 (2012).
[22] J. S. Patel and R. B. Meyer, Flexoelectric Electro-Optics of a Cholesteric Liquid Crystal, Phys. Rev. Lett. **58**, 1538 (1987).
[23] J. S. Patel and S.-D. Lee, Fast linear electrooptic effect based on cholesteric liquid crystals, J. Appl. Phys. **66**, 1879 (1989).
[24] A. Shapere and F. Wilczek, Classical Time Crystals, Phys. Rev. Lett. **109**, 160402 (2012).
[25] H. Watanabe and M. Oshikawa, Absence of Quantum Time Crystals, Phys. Rev. Lett. **114**, 251603 (2015).
[26] N. Y. Yao and C. Nayak, Time crystals in periodically driven systems, Phys. Today **71**, No. 9, 40 (2018).
[27] K. Sacha and J. Zakrzewski, Time crystals: A review, Rep. Prog. Phys. **81**, 016401 (2018).
[28] D. V. Else, C. Monroe, C. Nayak, and N. Y. Yao, Discrete time crystals, Annu. Rev. Condens. Matter Phys. **11**, 467 (2020).
[29] S. Choi, J. Choi, R. Landig *et al.*, Observation of discrete time-crystalline order in a disordered dipolar many-body system, Nature (London) **543**, 221 (2017).
[30] N. Éber, P. Salamon, and Á. Buka, Electrically induced patterns in nematics and how to avoid them, Liq. Cryst. Rev. **4**, 101 (2016).
[31] N. V. Madhusudana and R. Pratibha, Electromechanical coupling in cholesteric liquid crystals, Mol. Cryst. Liq. Cryst. Lett. **5**, 43 (1987).
[32] M. R. Kuzma, Nonequilibrium Periodic Structures Induced by Rotating and Static Fields in a Lyotropic Nematic Liquid Crystal, Phys. Rev. Lett. **57**, 349 (1986).
[33] S. Kaur, A. Belaissaoui, J. W. Goodby, V. Görtz, and H. F. Gleeson, Nonstandard electroconvection in a bent-core oxadiazole material, Phys. Rev. E **83**, 041704 (2011).
[34] B. X. Li, V. Borshch, and R. L. Xiao, S. Paladugu, T. Turiv, S. V. Shiyanovskii, and O. D. Lavrentovich, Electrically driven three-dimensional solitary waves as director bullets in nematic liquid crystals, Nat. Commun. **9**, 2912 (2018).
[35] L. Boyle, J. Y. Khoo, and K. Smith, Symmetric Satellite Swarms and Choreographic Crystals, Phys. Rev. Lett. **116**, 015503 (2016).
[36] D. Lee, H. Lee, L. K. Migara, K. Kwak, V. P. Panov, and J.-K. Song, Widely tunable optical vortex array generator based on grid patterned liquid crystal cell, Adv. Opt. Mater. **9**, 2001604 (2020).